Novelty

New multielement flexible matrix-matched calibration by urolith fine-grained pellets was developed and applied to quantify elemental maps in uroliths by LA-ICP-MS.

Preparation and testing of phosphate, oxalate and uric acid matrix-matched standards for accurate quantification of 2D elemental distribution in kidney stones sections using 213 nm nanosecond laser ablation inductively coupled plasma mass spectrometry

M. Vašinová Galiová,[a,b] K. Štěpánková,[a] R. Čopjaková,[c] J. Kuta,[d] L. Prokeš,[a,e] J. Kynický[f] and V. Kanický[a,b]

[a] Department of Chemistry, Faculty of Science, Masaryk University, Kotlářská 2, 611 37 Brno, Czech Republic

[b] Central European Institute of Technology (CEITEC), Masaryk University, Kamenice 5, 625 00 Brno, Czech Republic

[c] Department of Geological Sciences, Faculty of Science, Masaryk University, Kotlářská 2, 611 37 Brno, Czech Republic

[d] Research Centre for Toxic Compounds in the Environment (RECETOX), Masaryk University, Kamenice 126/3, 625 00 Brno, Czech Republic

[e] Department of Physical Electronics, Faculty of Science, Masaryk University, Kotlářská 2, 611 37 Brno, Czech Republic

[f] Department of Pedology and Geology, Faculty of Forestry and Wood Technology, Mendel University in Brno, Zemědělská 3, 613 00 Brno, Czech Republic

Abstract

Matrix-matched calibration for quantitative elemental mapping of kidney stones by laser ablation-inductively coupled plasma-mass spectrometry (LA-ICP-MS) was developed with a 213 nm Nd:YAG laser ablation device and a quadrupole mass spectrometer. The method was applied to the imaging of P, Na, Sr, Zn, Ba and Pb distributions over the section of the kidney stone specimen containing phosphate and oxalate phases. Eighteen kidney stone specimens consisting of phosphate, oxalate and urate phases in various proportions were cut into halves for both preparation of calibration pellets and bulk analysis. Homogeneity of calibration pellets was examined by scanning electron microscopy (SEM) and LA-ICP-MS, concluding that areas of individual biominerals were thoroughly mixed and their size in units of micrometers was well below the size of the used laser spot. Calcium was employed as internal reference element, being present in sufficient contents in studied kidney stones. Mean values of calcium contents in oxalate and phosphate phases separately were determined by electron microprobe (EMP) in the kidney stone section further subjected to the mapping. The actual (time- and space-resolved) Ca sensitivity was computed for each $^{44}Ca^+$ signal and used as internal reference for LA-ICP-MS isotopic signals of P, Na, Sr, Zn, Ba and Pb when mapping. Dependences of particular isotopic signal intensity/Ca sensitivity ratios *vs* average elemental contents by solution analysis were processed by ordinary least squares linear regression. Despite variable matrix the regression yielded calibration lines with insignificant intercepts, coefficients of determination $R^2 > 0.9955$, and relatively narrow prediction and confidence bands. However, in addition, the applicability of four-point calibration and four single-point calibrations as less time-consuming options was examined on the basis of the NIST SRM 1486 bone meal pellet analysis. Best fit was obtained for the four-point calibration and single-point calibration with phosphate pellet. Quantitative elemental maps of the kidney stone section were recorded and computed for P, Na, Sr, Zn, Ba and Pb. Feasibility of quantification by matrix-matched single-point calibration was verified by

determination of the median elemental contents in phosphate and oxalate phases by LA-ICP-MS and their arithmetic comparison mean values obtained over the same section area using EMP.

Introduction

Laser ablation-inductively coupled plasma-mass spectrometry (LA-ICP-MS) has already been employed in various fields of scientific research such as biology[1-4], medicine[5-9], geology[10-11], archaeology[12-17], etc. An ability to focus the laser beam onto a sample area with size from units to thousands of square micrometers together with limits of detection down to units of milligrams per kilogram make this method interesting for elemental mapping in "microscale". For example, elemental distribution was studied in archaeological findings, such as tooth and bone tissues, in order to reveal diet and migration/mobility[15-17] of ancient population. Results of analyses of recent samples are used in biomedicine and archaeology [18-21]. Similarly, fish scales and otoliths as indicators of migration of fish, environmental pollution, water salinity and temperature were analysed[22, 23]. LA-ICP-MS is a suitable technique to investigate phytoremediation where the knowledge about deposition of toxic element is required[1-4]. Considerable interest of scientific community is focused on the monitoring of elemental distribution in soft tissues such as brain, muscle, kidney tissue, tumors etc., or on a single cell analysis[24-27]. Where elements of interest are stored, how their presence affects the distribution of other elements and how they relate to specific disease – those are the questions that might be answered by LA-ICP-MS analysis.

The chemical and mineralogical composition of a kidney stone is related to a particular disease which is associated with a specific kidney stone formation, depends on medical treatment and diet of a patient, metabolic conditions, and is influenced by environmental pollution of an area of patient´s domicile and workplace. Chemical analysis might be helpful in understanding kidney stone formation, growth, and medical treatment. In general, kidney stone (urolith) has miscellaneous mineralogical composition, and phosphate, oxalate, carbonate, uric acid, cysteine, xanthine are the main matrices. Correspondingly, several variants of minerals are present, e.g., in case of phosphate we find struvite $MgNH_4PO_4 \cdot 6H_2O$, brushite $CaHPO_4 \cdot 2H_2O$, whitlockite $Ca_9(MgFe)(PO_4)_6PO_3OH$, and apatite ($Ca_5(PO_4)_3(OH,F,Cl)$) with variable portion of OH^- (hydroxylapatite), F^- (fluorapatite) and CO_3^{2-} (carbonate-hydroxylapatite) anions. The oxalate occurs as whewellite $Ca(C_2O_4) \cdot H_2O$ and weddellite $Ca(C_2O_4) \cdot 2H_2O$. The urate matrix can be present as uric acid $C_5H_4N_4O_3$, or uric acid dihydrate $C_5H_4N_4O_3 \cdot 2H_2O$ and its salts, such as ammonium urate $NH_4C_5H_3N_4O_3$, sodium urate monohydrate $NaC_5H_3N_4O_3.H_2O$. Usually, a urolith contains more than one mineral and therefore, direct analysis of solid sample is preferred in order to preserve spatial information [28-30].

Various techniques have been routinely employed in mineralogical and surface analysis of kidney stones, such as infrared spectroscopy [31, 32], Raman spectroscopy [32, 33], X-ray diffraction [34, 35], tomography[36], polarization optical crystallography, chemical microscopy, ultraviolet-visible spectroscopy and photomicroscopy, and light microscopy for macroscopic and microscopic examination. Besides, scanning electron microscopy (SEM/EDX) [37] or laser induced breakdown spectrometry (LIBS) [38, 39] were used for surface analysis. Exploratory study focused on possibilities of calibration by pressed pellets prepared from uroliths for bulk analysis and microanalysis by LIBS, laser ablation - laser induced breakdown spectrometry (LA-LIBS) and LA-ICP-MS/OES brought comparison

of calibration curves in terms of linearity and coefficients of determination. However, no elemental mapping of uroliths was attempted [40].

However, when information on spatial distribution of trace and minor elements is required, some of above methods do not meet requirements on limits of detection (LOD). The LA-ICP-MS combines an appropriate resolution in tens of micrometers of the laser spot diameter with values of LOD in units of mg kg^{-1} for most elements. So far only two papers have been already published on qualitative surface analysis of kidney stones by LA-ICP-MS [41, 42]. A qualitative elemental mapping of uroliths by LA-ICP-MS and electron microprobe (EMP) imaging by means of backscattered electrons (BSE) were applied to distinguish particular mineral phases. Bulk analysis of selected elements in oxalate and phosphate phases by LA-ICP-MS was based on calibration with NIST SRM 1486 (bone meal) and confirmed by EMP analysis, however no quantitative elemental maps were created.[42]

Major problem of LA-ICP-MS quantification consists in lack of reliable, commercially available calibration material. In such case, an effort is devoted to preparation of laboratory-made standards. As examples, a spiked gelatine[43], agarose[44] or tissue freezing medium[1] are presented for calibration of the LA-ICP-MS determination of metals/metalloids in soft tissues. The calibration can be based on commercially available standards with similar matrix, which are spiked with required analytes [2]. If a suitable reference material is not available, and gelatine or agarose do not match properties of analysed samples, real samples with similar matrix, previously analysed by independent methods, may be used with or without spiking[5, 46]. If material properties allow, the sample is crushed, milled, homogenized and the resulting powdered material is pressed into the pellet[47] or mixed with the matrix prepared by sol–gel technique with subsequent homogenization and pelletization[48-50]. Another approach consists in pressing of powdered sample with some suitable binder[17, 50].

Uroliths are usually constituted by several mineral phases that are present in various proportions and differ in physical and physico-chemical properties. Consequently, different ablation rates exist in particular mineral zones and make quantitative elemental mapping by LA-ICP-MS difficult unless signal correction by a suitable internal reference is employed. Similarly, such a calibration is necessary which covers appropriately wide ranges of elemental contents and therefore, particular calibration standards would contain various proportions of minerals, and trace elements on various content levels. It is obvious that no compact calibration material is available and calibration has to be based on pressed powdered pellets.

Preparation of powdered calibration standards has been known for decades as it was being used for emission spectrography with electric arc excitation and X-ray fluorescence spectrometry. Calibration standards were typically prepared by mixing of solid powdered reagents or natural previously analysed materials with subsequent homogenization of resulting mixtures. As both the spectral analytical methods exhibit non-spectral interferences, matrix-matched calibration with internal reference was indispensable for quantitative analysis.

An easier way how to prepare matrix-matched calibration standards for LA-ICP-MS elemental mapping of urolith sections is the use of already analysed urolith samples, properly crushed, milled, homogenized and pressed, instead of mixing of individual chemical reagents. In comparison with spectrography or X-ray fluorescence spectrometry of powdered materials, quantitative elemental mapping of uroliths by LA-ICP-MS comprises another factor, namely the difference between properties of calibration standards and analysed samples. Different ablation rate would exist not only between minerals, but also between pressed pellets and surface of urolith sections. Therefore, reliable internal reference is necessary to compensate for these multiple effects.

No quantitative LA-ICP-MS elemental maps of uroliths have been published so far. In the work [40], calibration capabilities of laser ablation based techniques were studied for the purpose of kidney stones bulk analysis and microanalysis. Intentionally the coarse-grained pellets were prepared from kidney stones instead of finely ground ones, thus respecting uroliths original heterogeneity and multiphase matrix structure consisting of several biominerals. This approach has been used because especially LIBS and LA-LIBS are more prone to matrix effects than LA-ICP-OES/MS. Thus, urolith structure partially preserved in coarse-grained pellets might alleviate the differences between such pellets and kidney stone sections in case of possible future elemental mapping. To eliminate coarse-grained pellet heterogeneity, a large ablated area and signal averaging were employed. As a result, linear relationship between content and signal was obtained, however, only loose correlation was observed, especially for LIBS. Moreover, mineralogical composition influenced preparation and mechanical properties of coarse-grained pellets. Pellet cohesion and strength depended on prevailing phase (phosphate, oxalates, urates), which significantly influenced target material removal by laser beam. Discussed work [40] is focused only on the comparison of laser ablation based methods in terms of calibration and does not address elemental mapping. The hole drilling, from the viewpoint of mapping a time-consuming ablation mode, was employed for this calibration study.

In the work [42] qualitative elemental distributions over urolith sections were obtained by LA-ICP-MS and particular biomineral zones were identified using the EMP/BSE. Influence of different ablation rates on LA-ICP-MS signal magnitude in various mineral phases was compensated by applying sensitivity of calcium isotope as internal reference, for which average content of calcium was determined in individual phases by EMP. Elemental associations to mineral phases distinguished by Ca/P signal ratio were derived based on LA-ICP-MS signal distributions compensated for different ablation rates. Calibration with single pressed pellet prepared from NIST SRM 1486 bone meal was employed for bulk analysis of oxalate and phosphate mineral phases and confirmed by analysis of average composition by EMP.

As already stated, only qualitative 2D distribution of isotope signals has been published [41, 42] or calibration based on pressed coarse-grained urolith pellets suited rather for LIBS has been developed but not tested for elemental mapping [40]. Single standard calibration with NIST SRM 1486 has been used for determination of average composition of mineral phases but not for quantification of elemental maps [42]. Although it appeared that NIST SRM 1486 can be used to quantify these distributions [42], there remains the scope for increasing reliability of the calibration.

Several reasons exist to substitute real matrix-matched calibration samples for the NIST SRM 1486. Contents of some elements are significantly higher in uroliths than in the NIST SRM 1486 which results in inappropriate extrapolation with respect to the calibrated range. This applies to most analytes considered in this work (SRM *vs* sample: 0.47 %$_{m/m}$ Mg *vs* 10 %$_{m/m}$ Mg, 0.50 %$_{m/m}$ Na *vs* 1.50 %$_{m/m}$ Na, 264 mg kg^{-1} Sr *vs* 500 mg kg^{-1} Sr, 147 mg kg^{-1} Zn *vs* 1000 mg kg^{-1} Zn, 1.3 mg kg^{-1} Pb *vs* 20 mg kg^{-1} Pb). In the NIST SRM 1486 only contents of Ca, P, Mg, Fe, Pb, K, Sr and Zn are certified, while contents of Si, Na, C, Al, As, Cd, Cu, F, Mn and Se are provided as additional information. Therefore, especially in case of traces (Al, As, Cd, Cu, Mn, and Se) it would be advisable to verify their contents in a particular SRM package by solution analysis. Available indicative values of elemental contents in the SRM are too low (mg kg^{-1}: < 1 Al, 0.006 As, 0.003 Cd, 0.8 Cu, 1 Mn, 0.13 Se). Data on the level of contents of other important (potentially toxic) trace elements (Ni, Cr, Hg) are missing in the SRM certificate. Finally, the NIST SRM 1486 represents only calcium phosphate matrix, while kidney stones contain more minerals.

The aim of this study consists in developing a new, flexible matrix-matched calibration for LA-ICP-MS quantification of 2D elemental distributions in urolith sections. Fine-grained urolith pellets are considered for calibration to minimize heterogeneity and improve LA-ICP-MS signal stability. Eighteen urolith samples comprising concrements which consist of phosphate, oxalate and urate phases are included in the calibration study in order to encompass majority of types of analysed kidney stones and ranges of possible elemental contents. Maximum number of calibration samples is employed for construction of calibration curves at first, and linearity as well as presence of outliers due to possible influence of matrix is statistically tested. For practical reasons, one four-point calibration and four single-point calibrations are tested, too. The procedure consists in: *i)* making of calibration kit of pressed pellets prepared from uroliths, *ii)* study of homogeneity and signal stability during laser ablation, *iii)* construction of calibration curves of P, Na, Sr, Zn, Ba and Pb, *iv)* verification of matrix-matched calibrations by analysis of NIST SRM 1486, and finally *v)* quantification of 2D elemental distributions and verification of results using EMP.

Experimental

Mineralogical composition of uroliths

A set of laboratory-made calibration standards and solid sample used for testing of prepared standards consists of surgically removed human kidney stones coming from a vast collection (more than eleven thousand uroliths) assembled by geologist Prof. Petr Martinec (Institute of Geonics, Academy of Sciences of the Czech Republic, Ostrava, Czech Republic). These uroliths have been obtained after the treatment of patients in the University Hospital Ostrava. The selection of uroliths appropriate for matrix-matched calibration was based on information about their mineralogical composition which was determined by infrared spectrometry. The calibration should include prevailing urolith matrices, which are phosphates, oxalates and uric acid, and therefore uroliths containing mainly phosphates (9 samples), uroliths consisting essentially of oxalates (5 samples) and uroliths composed of a mixture of uric acid and oxalates (4 samples) were selected for preparation of pressed powder pellets (Table 1). The sample no. 11605 was subjected to elemental quantification of 2D maps using matrix-matched pellets.

Phosphate matrix consists predominantly of apatite $Ca_5(PO_4)_3(OH,F,Cl)$ and struvite $NH_4MgPO_4 \cdot 6H_2O$ in various proportions. Oxalate matrix comprises whewellite $CaC_2O_4 \cdot H_2O$ and weddellite $CaC_2O_4 \cdot 2H_2O$. A separate group includes mixed kidney stones containing minor portion of oxalates (either whewellite or weddellite, exceptionally both) and uric acid ($C_5H_4N_4O_3$).

5

Table 1 Infrared spectrometry analysis of kidney stones employed for preparation of calibration pellets and for elemental mapping of urolith section (sample no. 11605).

Sample no.	Main matrix	Content of mineral (%$_{m/m}$)				
		Apatite	Struvite	Whewellite	Weddellite	Uric acid
5056	Ph	50	40	~	10	~
5255		70	20	~	10	~
5397		5	95	~	~	~
5996		35	65	~	~	~
6489		50	50	~	~	~
6671		70	20	~	10	~
6686		60	40	~	~	~
8393		55	55	~	~	~
9130		50	50	~	~	~
5166	Ox	25	~	75	1	~
6275		10	~	80	10	~
7851		5	~	95	~	~
8365		15	0	60	25	~
9081		5	~	95	~	~
11605		30	~	40	30	~
6432	UA	~	~	40	~	60
6585		~	~	5	5	90
7301		~	~	~	10	90
8500		~	~	~	20	80

Ph = phosphate matrix, Ox = oxalate matrix, UA = uric acid

Elemental composition of uroliths

Average content of the elements of interest in uroliths was determined using a wet digestion procedure followed by an ICP-MS measurement. Carbon content was determined by elemental analysis using a LiquiToc II device with Solids Module (Elementar Analysensysteme GmbH, Hanau, Germany). Elemental composition (Ca, Mg, C, P, Na, Sr, Zn, Ba and Pb) is summarized in Table 2. According to work [53] examined urolith samples contain also trace contents of Al, K, Cr, Mn, Fe, Co, Ni, Cu, Se Rb, Zr, Mo, Cd, Sn and Hg. The ICP-MS and carbon analyses were performed at the laboratory of Research Centre for Toxic Compounds in the Environment, Faculty of Science, Masaryk University, Brno, Czech Republic. Both analytical procedures have already been reported elsewhere.[51, 53] The results of solution ICP-MS analysis slightly differ in some cases from those of IR screening, which probably results from the fact that each of the halves of a particular kidney stone was crushed and homogenized separately with the assumption that a kidney stone is approximately radially symmetric.

Table 2 Contents of selected major, minor and trace elements in studied kidney stones obtained by ICP-MS solution analysis.

Sample no.	Main matrix	Elemental content $\%_{m/m}$				
		Ca	Mg	C	P	Na
5056		23.6 ± 0.8	4.28 ± 0.09	3.29 ± 0.09	17.7 ± 0.4	0.63 ± 0.01
5255		23.8 ± 0.8	4.07 ± 0.09	3.02 ± 0.08	17.5 ± 0.4	0.96 ± 0.02
5397		0.35 ± 0.01	10.1 ± 0.2	1.06 ± 0.03	14.3 ± 0.3	0.0223 ± 0.0004
5996		12.8 ± 0.4	6.5 ± 0.1	2.84 ± 0.08	15.2 ± 0.3	0.69 ± 0.01
6489	Ph	18.3 ± 0.6	4.8 ± 0.1	2.92 ± 0.08	16.4 ± 0.3	0.91 ± 0.01
6671		27.5 ± 0.9	2.60 ± 0.05	3.6 ± 0.1	18.3 ± 0.4	1.52 ± 0.02
6686		21.1 ± 0.7	4.7 ± 0.1	3.52 ± 0.09	17.5 ± 0.4	0.81 ± 0.01
8393		20.1 ± 0.6	5.1 ± 0.1	2.29 ± 0.06	16.7 ± 0.4	0.67 ± 0.01
9130		23.2 ± 0.7	3.90 ± 0.08	2.82 ± 0.08	16.8 ± 0.4	0.62 ± 0.01
5166		26.5 ± 0.8	0.061 ± 0.001	11.5 ± 0.3	2.05 ± 0.04	0.223 ± 0.004
6275		26.4 ± 0.8	0.0404 ± 0.0008	11.4 ± 0.3	1.50 ± 0.03	0.151 ± 0.002
7851	Ox	24.5 ± 0.8	0.0280 ± 0.0006	11.9 ± 0.3	0.339 ± 0.007	0.135 ± 0.002
8365		25.9 ± 0.8	0.115 ± 0.002	8.6 ± 0.2	2.63 ± 0.06	0.111 ± 0.002
9081		24.5 ± 0.8	0.0231 ± 0.0005	10.9 ± 0.3	0.227 ± 0.005	0.086 ± 0.001
11605		27.3 ± 0.9	0.160 ± 0.003	9.8 ± 0.3	5.0 ± 0.1	0.258 ± 0.004
6432		1.33 ± 0.04	0.00288 ± 0.00006	26.6 ± 0.7	0.0360 ± 0.0008	0.0214 ± 0.0003
6585	UA	0.076 ± 0.002	0.00080 ± 0.00002	27.2 ± 0.7	0.0138 ± 0.0003	0.0133 ± 0.0002
7301		0.31 ± 0.01	0.00134 ± 0.00003	23.6 ± 0.7	0.0191 ± 0.0004	0.0428 ± 0.0007
8500		0.97 ± 0.03	0.00240 ± 0.00005	24.9 ± 0.7	0.0212 ± 0.0004	0.014 ± 0.0002
Sample no.	Main matrix	Elemental content mg kg^{-1}			
		Sr	Zn	Ba	Pb
5056	Ph	314 ± 16	251 ± 5	10.1 ± 0.3	10.4 ± 0.3
5255		309 ± 15	939 ± 17	14.4 ± 0.4	67 ± 2

7

5397	4.4 ± 0.2	29.0 ± 0.5	0.72 ± 0.02	0.324 ± 0.008
5996	122 ± 6	373 ± 7	3.3 ± 0.1	9.7 ± 0.2
6489	180 ± 9	458 ± 8	4.1 ± 0.1	3.02 ± 0.08
6671	415 ± 21	711 ± 13	24.3 ± 0.8	13.8 ± 0.3
6686	329 ± 16	945 ± 17	12.3 ± 0.4	51 ± 1
8393	181 ± 9	477 ± 9	11.3 ± 0.4	19.0 ± 0.5
9130	517 ± 26	590 ± 11	22.4 ± 0.7	5.9 ± 0.1
5166	63 ± 3	137 ± 2	2.05 ± 0.06	9.6 ± 0.2
6275	38 ± 2	180 ± 3	0.84 ± 0.03	19.6 ± 0.5
7851	33 ± 2	31.0 ± 0.6	0.54 ± 0.02	5.1 ± 0.1
8365 Ox	102 ± 5	280 ± 5	9.7 ± 0.3	7.8 ± 0.2
9081	31 ± 2	45.4 ± 0.8	1.04 ± 0.03	5.4 ± 0.2
11605	116 ± 6	534 ± 10	5.0 ± 0.2	27.9 ± 0.7
6432	1.72 ± 0.09	9.7 ± 0.2	0.17 ± 0.01	0.349 ± 0.009
6585	0.081 ± 0.004	7.0 ± 0.1	0.066 ± 0.002	0.58 ± 0.01
7301 UA	1.17 ± 0.06	3.05 ± 0.05	0.052 ± 0.002	0.179 ± 0.004
8500	4.3 ± 0.2	6.7 ± 0.1	0.199 ± 0.006	0.83 ± 0.02

Ph = phosphate matrix, Ox = oxalate matrix, UA = uric acid

Making of pellet

Eighteen uroliths were employed for preparation of matrix-matched calibration standards (Table 1, samples no. 5056 - 9130). Making of pellets presents an essential critical step in terms of precision and accuracy of LA-ICP-MS measurement. In particular, the homogeneity of the pellets and the grain size are crucial prerequisites to achieve a stable LA-ICP-MS signal. Besides, sufficient pellet cohesion is necessary to minimize cracking and crumbling of material at ablation.

The use of pellets prepared from finely ground kidney stones was aimed at homogenizing multiphase composition of uroliths to reduce possible spread of calibration points. Kidney stones considered for pellet preparation were crushed in agate bowl and subsequently milled and homogenized in a ball mill (Planetary Micro Mill Pulverisette 7, FRITSCH; Germany). One portion of each pulverized sample was pressed without adding any binder into pellets with diameter of 12 mm and 2 mm thickness. Pelletization was performed for 30 s at the pressure of 1.3 GPa using a manual hydraulic press (Mobiko Company, Czech Republic). The remaining powdered sample was dissolved for subsequent ICP-MS analysis.

In contrast to coarse-grained pellets, which were applied to study of calibration capabilities in LIBS, LA-LIBS, LA-ICP-OES/MS methods [40], the fine grained ones eliminated the lack of pellet cohesion. The difference in particle size was significant. While scanning electron microscope (SEM) exposures of intact and ablated coarse-grained pellets in [40] show particle size between 10-50 μm and in some cases even above 100 μm, SEM images in this work (Fig. 1) show particles around 1 μm, i.e., about one or two orders of magnitude smaller.

Preparation of urolith section for elemental mapping

For LA-ICP-MS elemental mapping of urolith section surface, sample no. 11605 was cut into two parts using a diamond saw and one part of the urolith was mounted into polymethylmetacrylate (PMM) and polished. The other part was pulverized and left for the determination of average composition.

Laser ablation-inductively coupled plasma-mass spectrometry procedures

Laser ablation experiments were performed at the Laboratory of Atomic Spectrochemistry, Department of Chemistry, Faculty of Science, Masaryk University. A pulsed Nd:YAG laser system UP 213 (New Wave Research, Inc., Fremont, CA, USA) working at 213 nm and a pulse duration of 4.2 ns was used. The ablation system is equipped with a SuperCell (New Wave Research) designed to enable rapid eluting of the ablation-generated aerosol in a large format cell. Helium was used as a carrier gas with the flow rate of 1 L min^{-1}. Aerosol was transported from the ablation cell using a 1-m long polyurethane transport tube (i.d. of 4 mm) to the ICP (ICP-MS Agilent 7500ce, Agilent Technologies, Santa Clara, CA, USA). The instrument was operated with collision cell in He-mode for minimization of possible polyatomic interferences.

The urolith section (no. 11605) and calibration pellets were rastered with the square-shaped laser beam (65 μm) in line scanning mode at the scan speed of 40 μm s^{-1} at the fluence of 7.5 J·cm^{-2} and the laser repetition rate of 5 Hz. Rasters composed of an appropriate number of parallel lines and spaced apart 100 μm were employed. The operating parameters are summarized in Table 3. Calibration sets were designed and statistically tested for P, Na, Sr, Zn, Ba and Pb, while Ca was employed as internal reference. LA-ICP-MS data were collected also for carbon as matrix element, for Mg as medium/minor element, for K as minor/trace element and for Al, Mn, Fe, Cu, Rb, and Sn as trace elements. Significantly different content in various types of uroliths was also found for Fe, Cu,

and Sn by ICP-MS solution analysis [53] which corresponded to a range of LA-ICP-MS signals measured in this work.

Table 3 Operating parameters of LA-ICP-MS, measured isotopes and acquisition times.

Laser ablation system	New Wave Research UP213
Laser	Nd:YAG
Ablation chamber	SuperCell
Wavelength	213 nm
Pusle duration	4.2 ns
Fluence	7.5 J cm^{-2}
Repetition rate	5 Hz
Carrier gas flow rate	He 1.0 L min^{-1} + Ar 0.6 L min^{-1}
Ablation mode	Line scan
Ablation spot size	65 µm (square)
Scan speed	40 µm s^{-1}
Distance between lines	100 µm (for mapping only)

ICP-MS	ICP-QMS, Agilent 7500ce
Rf power input	1500 W
Plasma gas flow rate	Ar 15.0 L min^{-1}
Auxiliary gas flow rate	Ar 1.0 L min^{-1}
Sampling depth	8 mm
Collision cell	He 2.5 mL min^{-1}
Acquisition time and isotopes monitored	0.1 s: $^{12,\,13}C^+$, $^{23}Na^+$, $^{27}Al^+$, $^{31}P^+$, $^{39}K^+$, $^{55}Mn^+$, $^{56,\,57}Fe^+$, $^{63}Cu^+$, $^{66,68}Zn^+$, $^{85}Rb^+$, $^{86,\,88}Sr^+$, $^{118}Sn^+$, $^{135,137}Ba^+$, $^{208}Pb^+$
	0.05 s: $^{24,\,26}Mg^+$
	0.01 s: $^{42,\,43,\,44}Ca^+$

Scanning electron microscopy study and electron microprobe analysis

The samples were examined by SEM and EMP prior to LA-ICP-MS experiments. Sample surface was carbon coated for the SEM and EMP study. The quality of pellets in respect to the grain size and phase homogeneity was inspected using SEM. The MIRA III SEM equipped with a back-scattered electrons (BSE) detector (laboratories of TESCAN, a. s., Brno, Czech Republic) was employed. Back-scattered electron images (1024 x 1024 pixels) were acquired under the following analytical conditions: an accelerating voltage of 20 kV and a beam current of 20 nA.

The chemical composition (including major and trace elements) of specific phases within the kidney stone sample no. 11605 was determined using a Cameca SX100 electron microprobe (Department of Geological Sciences, Masaryk University, Brno) to check trueness of results obtained by quantification of 2D elemental distribution *via* LA-ICP-MS. The instrument was operated at an accelerating voltage of 15 kV, a beam current of 6 nA and scanning beam mode over the area 20 x 15 µm. The following calibration standards and analytical lines were used: (Kα) lines: fluorapatite (Ca, P), albite (Na), sanidine (Si, Al, K), Mg_2SiO_4 (Mg), NaCl (Cl), hematite (Fe), gahnite (Zn), $SrSO_4$ (S) and topaz (F); (Lα) lines: $SrSO_4$ (Sr), baryte (Ba). The peak counting times ranged 10-20 s for major elements, and 20-80 s for minor elements. The matrix effects were corrected using the PAP routine.[52]

Results and discussion

Matrix-matched urolith standards

The homogeneity of pellets is of utmost importance for reliable LA-ICP-MS calibration. The critical case may be urolith containing a minor portion of mineral which substantially differs in chemical composition from the matrix mineral. Therefore, structure of pellets was inspected using SEM. As an example, pellet prepared from urolith no. 7851 containing 95 %$_{m/m}$ of oxalate and 5 %$_{m/m}$ of phosphate is discussed. The BSE large-scale image of the surface of this pellet does not indicate apparent lack of homogeneity, although bright grains consisting of phosphate and dark oxalate grains are easily distinguishable (Fig. 1 a). The detailed image demonstrates almost uniform distribution of phosphate-rich grains characterized by bright spots (<<1 µm) within dark oxalate area (Fig. 1 b). As the ablation event occurs on the area of (65 x 65) µm^2 (marked with square in Fig 1 b), the inhomogeneity in low micrometric scale is acceptable and would not result in the isotopic signal instability and biased results. Indeed, as it is obvious from Fig. 2 where three line scans over the surface of the pellet no. 7851 are recorded, the time-resolved signal of minor and trace elements such as Na (0.13 %$_{m/m}$), Sr (0.003 %$_{m/m}$), and Pb (0.0005 %$_{m/m}$) exhibits continuous course uninterrupted by any significant spike, which would otherwise indicate a time/space resolved ablation of a grain enriched with a particular element. This confirms a good "targeted" homogeneity, although these elements are predominantly associated with minor phosphates.[53]

Fig. 1 BSE images of 7851 pressed pellet surface (a) homogeneous character of pellet in large scale view, length of the scale 500 μm, (b) fine scale with evenly distributed phosphate (bright grains) within fine-grained oxalate matrix (dark color), length of the scale 20 μm, while the square outline defines the size of the laser beam spot (65×65 μm).
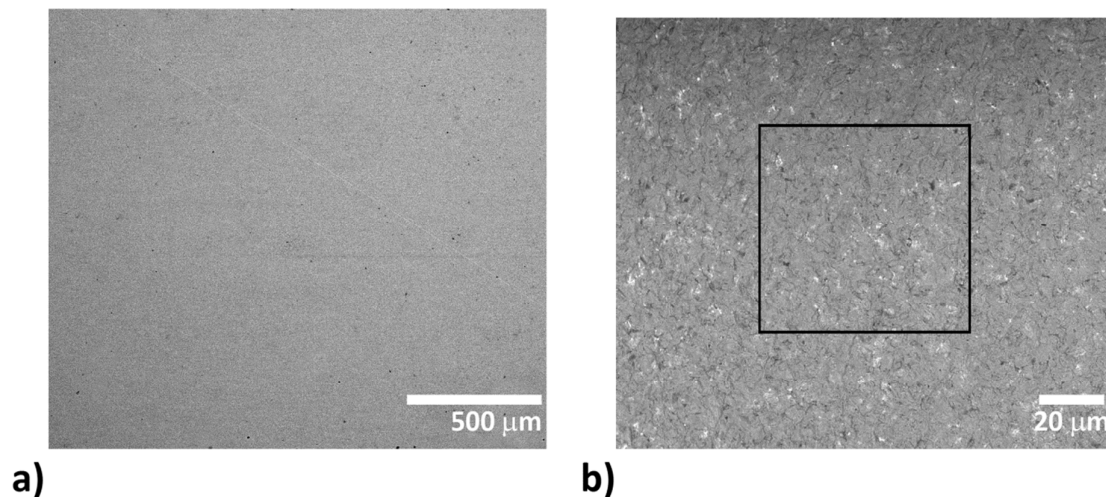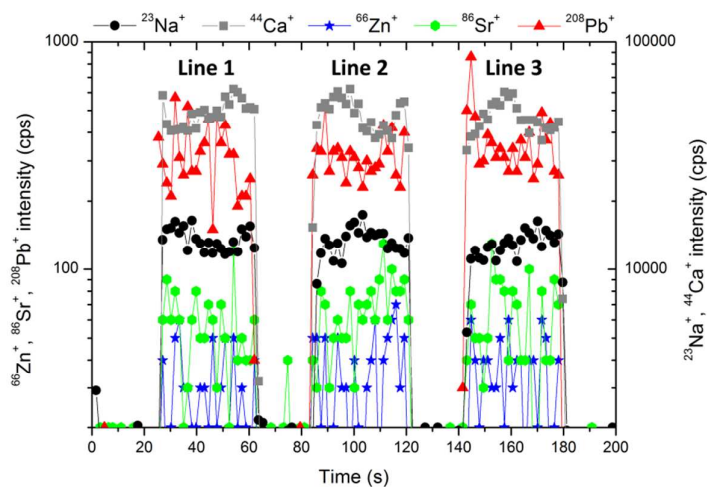

a)   b)

Fig. 2 The stability of the signal of $^{23}Na^+$, $^{44}Ca^+$, $^{66}Zn^+$, $^{86}Sr^+$, $^{208}Pb^+$ during the ablation of pellet no. 7851 within 3 lines with the length of 1.5 mm, approximately.

Compactness of pellets, their stability during ablation and relative insignificance of microinhomogeneity in comparison with the size of ablation spot in Fig. 1 b) can also be assessed on the basis of signal variability of main constituents. Major element contained in both phosphate uroliths (with the exception of the urolith no. 5397, which consist primarily of struvite) and oxalate uroliths is calcium (~12-27 % $_{m/m}$ Ca), while one of organic matrix elements in uric acid samples is carbon (~25 % $_{m/m}$ C), as it follows from Tables 1 and 2.

As phosphate pellets contain apatite and struvite in various proportions and also include ~10 % of weddelite in several cases, a fluctuation of $^{44}Ca^+$ signal along the line scans over the surface of a particular pellet indicates the degree of homogeneity of such a mixture and pellet compactness

(presence of cracks, crumbling by the interaction with a laser beam). The RSD of $^{44}Ca^+$ signal measured with all phosphate pellets falls within the range of 0.5-10.8 % for three ablation tracks located at different areas of the pellet surface. As an example, development of $^{44}Ca^+$ signal in time along mentioned ablation lines is shown for urolith pellet no. 7851 in Fig. 2. The oxalate pellets contain predominantly whewellite, while weddelite content ranges up to 25 % and phosphate minerals group constitutes from 5 to 30 % of the total. Signal variability of $^{44}Ca^+$ in oxalate pellets is characterized by RSD ranging from 0.6 to 4.9 %. Calcium is minor element (0.1 -1.3 %$_{m/m}$) in uric acid group uroliths, and therefore $^{44}Ca^+$ signal exhibits the most significant fluctuation with RSD between 4.4 % and 51 %. On the other hand, RSD of $^{12}C^+$ signal ranging from 3.3 to 7.1 % documents quite a good stability and homogeneity of uric acid pellets. Nevertheless, urate-based pellets exhibit the highest fluctuation of $^{12}C^+$ signal in comparison with phosphate (0.4-2.0 %) and oxalate (0.6-2.5 %) groups, which is probably due to the presence of some fine cracks on the pellet surface. The internal precision, which reflects the micro scale homogeneity, is expressed *as* median value of %RSD of $^{12}C^+$ isotopic signal fluctuation, and is equal to 4.5 %, 4.1 % and 9.9 % for groups of uroliths with prevailing phosphate, oxalate and urate matrices, respectively. It should be generally noted that calcium and carbon signal fluctuation reflects, besides pellet compactness and homogeneity of their distributions in all kinds of pellets, also both the influence of ablation rate variability and overall instrumental precision of the LA-ICP-MS system. Obviously, Ca and C signal stability can be considered an appropriate common indicator of a particular pellet quality and suitability for calibrating.

The occurrence of kidney stones with only one matrix is quite uncommon. It is not exception that more than two matrices can be found in uroliths. Therefore, we attempted to create a single calibration which would be applicable to various types of kidney stones. The concept of matrix-matched calibration in our approach means that a single calibration would be able to cover phosphate, oxalate and urate matrix. A necessary prerequisite for application of the common calibration is the same or at least close sensitivity for these matrices.

The pellets were divides into three groups according to their mineralogical composition: *i)* 9 pellets with predominant phosphate matrix; *ii)* 5 pellets with prevailing oxalate matrix; and *iii)* 4 pellets with the main content of uric acid (Table 1). The response in these three groups of uroliths was evaluated using $^{44}Ca^+$ signal. Sensitivity was calculated for each pellet as the ratio of $^{44}Ca^+$ net signal to Ca content in the pellet, the values in each group were averaged and standard deviations were calculated and plotted to (Fig 3), while sensitivities in oxalate and uric acid matrices were normalized to sensitivity in phosphate group. Thus, normalized sensitivity in phosphate group is equal to one. The Ca contents in pellets with phosphate and oxalate main constituents are both high and close, while the pellets with uric acid/oxalates contain only 0.1-1.3 %$_{m/m}$ Ca. As observed, the highest sensitivity was obtained for the group of phosphate-based pellets while the sensitivity in oxalate and uric acid pellets reaches 81 % and 96 % of that maximum value (Fig. 3). However, non-parametric Kruskal-Wallis test proved no statistically significant difference between sensitivities.

Fig. 3 Sensitivity of calcium isotopic signal in oxalate and uric acid matrices normalized to the sensitivity in phosphate, error bars represent standard deviation.
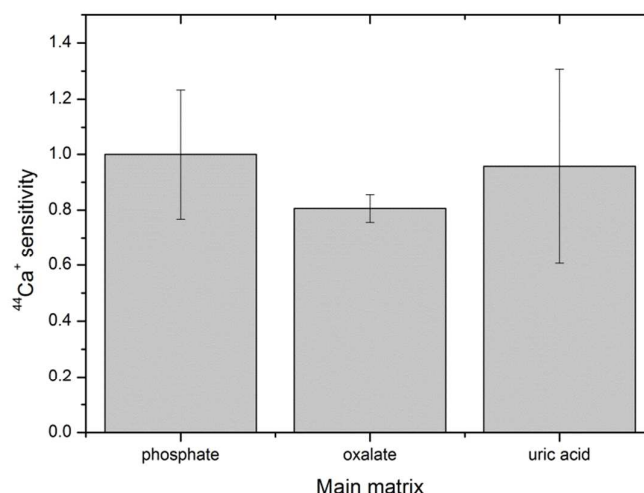
Development of matrix-matched calibration kits

Eighteen pellets prepared from urolith specimens listed in Table 1 were used for construction of calibration plots for P, Na, Sr, Zn, Ba and Pb. Calibration kits for particular analytes are listed in Table 4. Calibration for Mg of the same quality was obtained, too (not presented in this work). The LA-ICP-MS measurement was repeated three times on each pellet using three parallel lines with the length of 1.2 mm under conditions specified in experimental part. Background intensity was recorded prior to ablation and then subtracted from signal measured during ablation period. Sensitivity of $^{44}Ca^+$ signal was applied as internal reference for correction of matrix effects.

Calibration points were plotted as analyte signals divided by $^{44}Ca^+$ sensitivities *vs* elemental contents. Calibration curves were fitted using a computer program Origin. Linear regression models resulted from the tests and two sets of coefficients of determination (R^2) were computed; one set with all data points included, and the other after outliers had been eliminated (Table 4). In Fig. 4, calibration curves of P, Na, Sr, Zn, Ba and Pb are plotted together with confidence and prediction bands without outliers. Ordinary least squares linear regression was applied and the regression line was fitted for calibration points representing arithmetic means of 3 replicates for each pellet. Each replicate represents average value of all MS readings obtained during the line scan ablation measurement. Vertical error bars represent combined uncertainty of replicates calculated based on standard deviation of the signal of isotope (analyte) and standard deviation of calcium isotope signal (internal reference). Horizontal error bars represent uncertainty of ICP-MS solution analysis. Regression lines computed without outliers show tighter correlation, which is obvious from values of $R^2 > 0.99$, namely in the range 0.9955-0.9991 (Table 4). At this point it should be emphasized that calibrations for Sr, Mg, Ba, and Na obtained with coarse-grained pellets [40] exhibit worse values of R^2 (0,75 − 0.90). All calibration plots are described by equation $y = bx$ with zero value of intercept at the level of confidence $(1-\alpha) = 0.975$. The intercepts are not statistically significant regardless of whether the outliers are retained in the regression sets or excluded on the basis of statistical testing. The absence of intercepts together with the proved validity of linear models indicates that the internal reference compensates for different ablation rates associated with the three various mineral matrices, and thus eliminates systematic error. Calibration line for phosphorus was fitted only with data points for oxalate and uric acid pellets, while phosphate data points were omitted as phosphorus is the main constituent in phosphate uroliths. In Fig. 4, calibration curves of P, Na, Sr, Zn, Ba and Pb are plotted together with confidence and prediction bands without outliers. Limits of

detection were calculated as the triple standard error of regression divided by the slope of the regression line, $3s_{y/x}/b$, considering the zero value intercept. It has to be emphasized that limits of detection calculated through the calibration lines generally depend on both the number and distribution of calibration standards and are in principle higher than those (instrumental) obtained simply based on the triple of the standard deviation of LA-ICP-MS blank signal recorded when ablation is off. Consequently, the LOD values in Table 4 follow from regression calculations performed in the presented regression ranges, and are associated with concrete calibration lines displayed in Fig. 4, while LOD values at a particular mapping may differ.

Table 4 Calibration kits, coefficients of determination, and limits of detection.

Element	Calibration standards Ph/Ox/UA[a]	R^2 Outliers included	R^2 Outliers left out	Regression range $\%_{m/m}$	LOD $\%_{m/m}$
P	0/5/4	0.9991	0.9991	0.014-2.6	<0.1
Na	6/5/4	0.9936	0.9955	0.013-1.5	<0.1
Sr	6/4/4	0.9896	0.9960	0.0001-0.052	<0.004
Zn	6/4/4	0.9868	0.9966	0.0003-0.094	<0.007
Ba	7/4/4	0.9777	0.9957	0.05-24[b]	<2[b]
Pb	9/1/3	0.9861	0.9974	0.18-67[b]	<4[b]

[a] Ph = phosphate matrix, Ox = oxalate matrix, UA = uric acid matrix

[b] LOD in mg kg^{-1} calculated as the triple standard error of regression divided by the slope of the regression line, $3s_{y/x}/b$, considering the zero value intercept. For completeness of information, regression ranges are presented here while the actual calibrations are limited to values above LODs.

Fig. 4 Calibration lines for P, Na, Sr, Zn, Ba and Pb after statistical analysis and outliers exclusion.
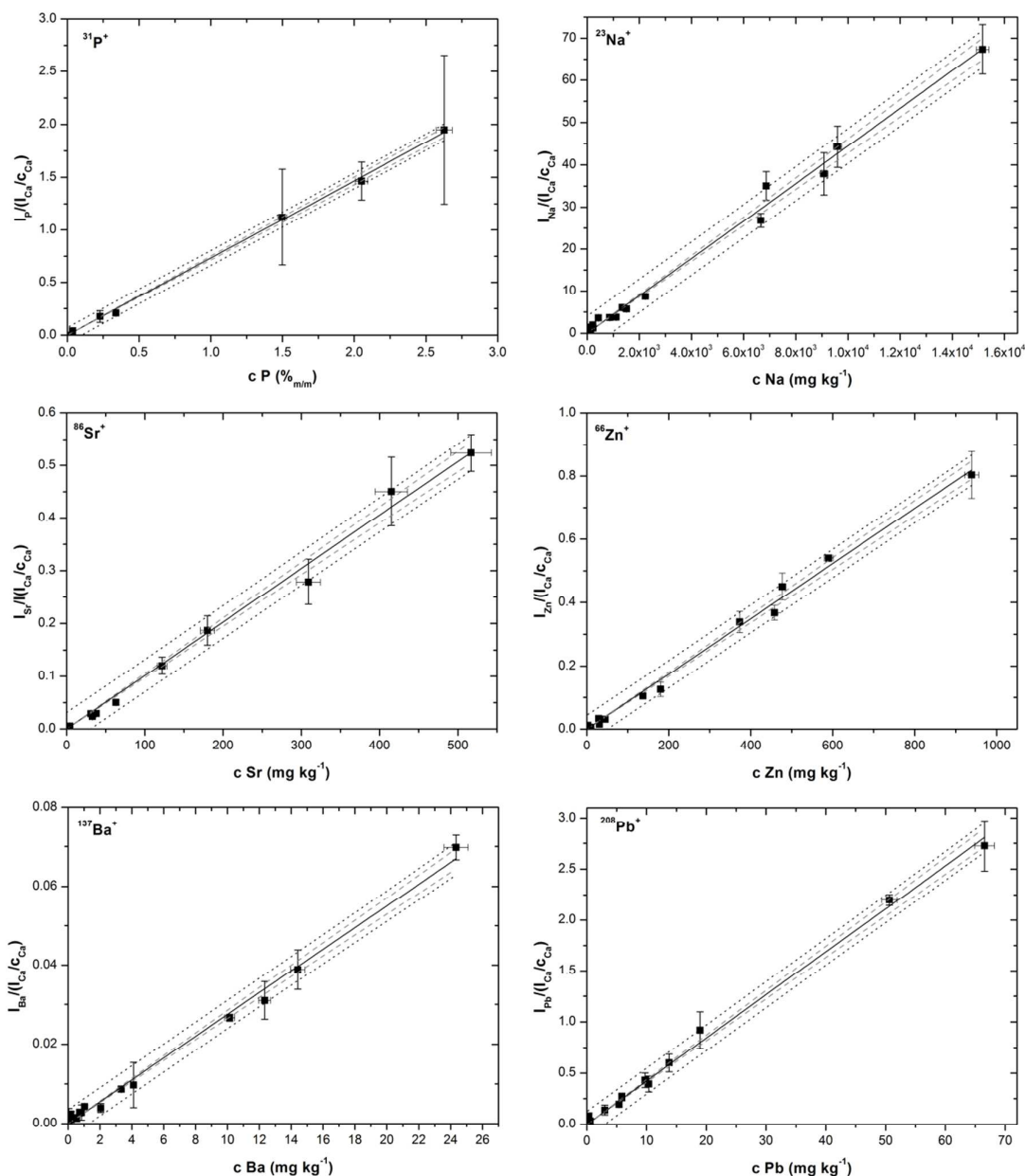
Verification of matrix-matched calibrations by analysis of NIST SRM 1486

Practical application of the presented calibration kits is limited by the size of the ablation cell (SuperCell), which holds only five pellets because the PMM block with the urolith section occupies a relatively large space (~5 cm^2). To minimize both the analysis time and the effect of handling the ablation cell on measurement stability, the calibration pellets and the urolith section should be inserted into the ablation cell at the same time. Based on the satisfactory results of the calibration dependence studies, we approached to explore the possibility of reducing the number of calibration points to four. In the extreme case, calibration with a single pellet would bring, besides reducing the time of analysis, in particular the possibility to place more samples for mapping into the ablation cell.

17

Therefore, four calibration pellets were selected to represent both the phosphate (3 pellets, 6686, 8393 and 9130) and the oxalate (1 pellet, 6275) matrix. The fifth pellet was the NIST SRM 1486, the bone meal, which was employed to prove whether the calibration kit is really matrix-matched, in the first approximation as regards the analysis of powdered material with phosphate matrix.

Ablation pattern applied to pellets consisted of ten parallel lines of the length of 2.8 mm. Measurement was performed under conditions specified in Experimental part. Two calibration procedures were examined: *i)* the four-point calibration comprising three phosphate and one oxalate pellet; *ii)* four single-point calibrations based on particular phosphate and oxalate pellets. Relative intensities representing ratios of signals of individual isotopes and the $^{44}Ca^+$ sensitivity were processed. Isotope $^{44}Ca^+$ sensitivity correlates reasonably with signals of analytes. This means that the internal reference follows analyte signal variations, which are due to both matrix-dependent ablation rate, and the fluctuations of instrumental operating conditions of the LA-ICP-MS system.

The NIST SRM 1486 elemental contents resulting from calibrations *i)* and *ii)* are shown together with the certified and published uncertified values in Table 5. Besides the four-point calibration with coefficient of determination in the range of 0.990-0.999, best fit is obtained with single-point calibrations using phosphate pellets, while oxalate matrix calibration leads to an underestimation of Ba content due to Ba content in pellet no. 6275 below LOD (Table 4). Similarly, Pb content in NIST 1486 is three times below LOD and cannot be determined under used method conditions. Finally, the calibration with phosphate pellet no. 9130 was selected for mapping of urolith section.

Table 5 Comparison of elemental contents with standard deviations in NIST SRM 1486 obtained with four-point and single-point calibrations after ablation of ten lines with the length of 2.8 mm, approximately.

Element	Certified values	Four-point calibration	6686 Phosphate	8393 Phosphate	9130 Phosphate	6275 Oxalate
			mg kg^{-1}			
P	12.30 ± 0.19 [a]	12.07 ± 0.68 [a]	12.06 ± 0.69 [a]	11.66 ± 0.66 [a]	12.19 ± 0.69 [a]	12.94 ± 0.74 [a]
Na	(0.50) [a, b]	0.48 ± 0.03 [a]	0.45 ± 0.02 [a]	0.34 ± 0.02 [a]	0.45 ± 0.02 [a]	0.32 ± 0.02 [a]
Sr	264 ± 7	273 ± 17	285 ± 18	274 ± 17	265 ± 16	269 ± 17
Zn	147 ± 16	148 ± 18	210 ± 17	153 ± 12	151 ± 12	128 ± 10
Ba	$189\text{-}314$ [c]	249 ± 12	235 ± 17	196 ± 14	227 ± 16	52.7 ± 3.8
Pb	1.335 ± 0.014	3.64 ± 0.48	2.68 ± 0.35	0.511 ± 0.068	0.99 ± 0.13	0.445 ± 0.059

[a] in %$_{m/m}$

[b] non-certified content

[c] the value is not included in the NIST SRM 1486 certificate; Ba content presented in the Table 5 is taken from Georem.[54]

19

Quantification of 2D elemental distributions

Besides the sensitivities of particular analytes measured in calibration pellets, the sensitivities of analytes obtained for sections of uroliths play an important role in quantification. Section of kidney stone exhibits different physical properties than the pressed pellet. Ablation rate depends on the mineral phase and its density and hardness. Consequently, different ablation rates in various minerals can be expected in a given urolith section in comparison with pressed pellet.

Elemental map of the part of the urolith no. 11605 section surface (1.4 × 1.9) mm^2 was quantified. The photograph of the whole sample surface with analyzed area marked with a rectangle is presented in Fig. 5 a. Sample no. 11605 contains 30 %$_{m/m}$ of phosphate and 70 %$_{m/m}$ of oxalate of which 40 %$_{m/m}$ is whewellite and 30 %$_{m/m}$ weddellite.

As shown in Fig. 5 b, the analyzed area is composed mainly of oxalate (whewellite > weddellite) and fluorapatite according to EMP analysis. Fluorapatite predominates in central part of kidney stone. Calculation of the structural formula from the results of EMP analysis indicates rather fine-grained mixture of predominant fluorapatite with minor amount of Mg-rich phosphate (probably struvite) than pure fluorapatite. Chemical heterogeneity of fluorapatite observed in BSE image reflects varying admixture of Mg-rich phosphate (higher amount of Mg-rich phosphate decreases brightness of BSE image). Fluorapatite is overgrown by fine-grained, colomorph oxalate, possibly weddellite. Coarse-grained compact oxalate, probably whewellite, predominates in kidney stone. The outermost part of kidney stone is composed of intergrowths of both types of oxalate (whewellite and weddellite). Contents of minor elements in whewellite and weddellite are similar and generally decrease from inner part of the kidney stone (close to the fluorapatite) to the rim.

Fig. 5 a) Photograph of no. 11605 kidney stone surface with marked area analyzed *via* LA-ICP-MS and EMP and b) BSE image marked surface with description of phases (Ph – phosphate and Ox - oxalate).

a)   b)
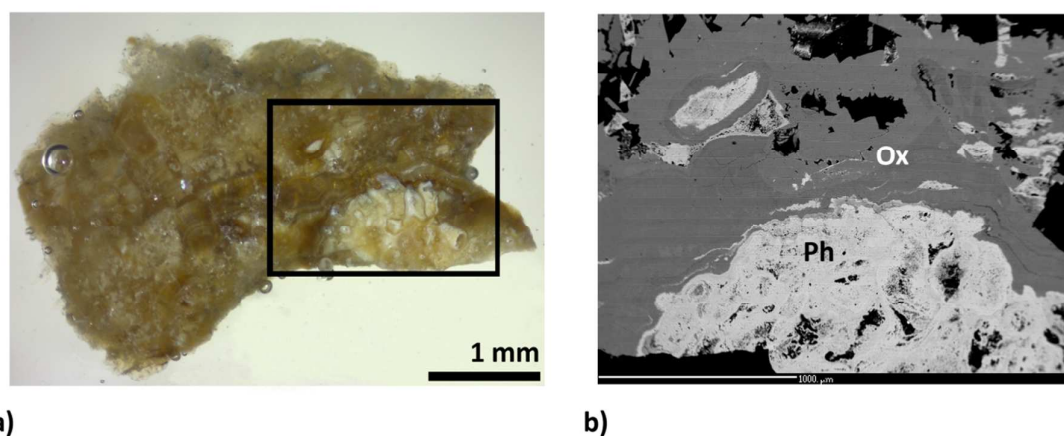
A single-point calibration was used with respect to low content of some elements in oxalate matrix and with the aim to reduce time of analysis. For this purpose, phosphate pellet no. 9130 was used as calibration standard.

Elemental 2D maps are shown in Fig. 6, where Ca distribution is presented on the level of intensities (Fig. 6 a), while P, Na, Sr, Zn, Ba and Pb (Figs. 6 b, c, d, e, f, g) are quantified. It should be noted right at the beginning that the quantification of inhomogeneous surface is hampered by the presence of defects (cracks) in phases. Besides, spatial resolution in the direction of x-axis is deteriorated by using the line scanning mode which induces overlapping of signals on the boundary

of phases. The spatial resolution of the elemental maps in the scanned area is also affected by the fact that lines are spaced 100 µm. As a result, the image of boundary is not sharp.

Quantification procedure is as follows. Prior to quantification, the signal corresponding to PMM resin was removed and thus filtered values were divided into two groups characterizing section areas. The area comprising $^{31}P^+$ signal corresponds exclusively to phosphate matrix whereas the area covered by $^{44}Ca^+$ signal defines the whole sample section surface as calcium is common for both oxalate and phosphate phases. This distinction allows quantifying elemental contents separately in particular phases.

A correction for different ablation rates in oxalate and phosphate matrix of the urolith section and in calibration pellets is of utmost importance for obtaining quantitative elemental distributions. The average ablation rate in phases of the sample section and in the pellet was determined on the basis of a large number of measurements. For this purpose, 50 and 80 values of $^{44}Ca^+$ signal in phosphate and oxalate phase were employed, respectively. Considering the Ca content in both phases obtained *via* EMP and median intensity values of $^{44}Ca^+$ for each of phases, the value of 1.3 was found which expresses that the Ca sensitivity in phosphate phase is higher in comparison with that in oxalate phase. In other words, ablation rate in oxalate reaches 80% of that in phosphate. This is in good agreement with a comparison of Ca sensitivities for pellets (Fig. 3). As a result, $^{44}Ca^+$ distribution (Fig. 6 a) corrected for difference in average ablation rate exhibits slightly higher intensity values in phosphate-rich domain, and intensity drops in small areas with material defects (cracks). The comparison of Ca (Fig. 6 a) and P (Fig. 6 b) distributions reveals that 42 % of the examined part of the section surface corresponds to phosphate matrix. It is apparent that found elemental distributions of Na, Sr, Zn, Ba and Pb (Figs. 6 c-g) are concentrated to area corresponding to phosphate-based matrix (Fig. 6 b).

Results of analyses of phosphate and oxalate phases in urolith no. 11605 are presented in Table 6. To verify that the quantification of 2D maps (Fig. 6), which is based on the pellet no. 9130, is not distorted by this single-point calibration, median values of elemental contents in both phases were also determined using three other single-point calibrations with pellets no. 6686, 8393 and 6275, employed for analysis of NIST SRM 1486. The range of thus obtained four median values is presented in Table 6 together with their arithmetic mean and corresponding standard deviation for each analyte. It is obvious from these low SD values that all the used single-pellet calibrations provide close results. Content variability over the phase area is expressed as the median absolute deviation (MAD), which is the median of the absolute deviations from the content´s median. The median was selected in order to minimize the influence of presence of cracks and distortion of signal by line scanning mode. For comparison, average values (arithmetic mean) with standard deviations are presented for EMP analyses of studied phases. However, contents of Ba and Pb in phosphate and Sr, Zn, Ba and Pb in oxalate are below LOD of EMP. The agreement between LA-ICP-MS and EMP results is satisfactory when considering the fact that the variability in elemental contents within phosphate and oxalate area phases reaches at least 32 % (P), 51 % (Na) and 44 % (Zn), respectively. As the quantification relies on the single-point calibration instead of the multi-point one, LODs of LA-ICP-MS measurement were calculated as the triple standard deviation of background intensity divided by sensitivity were following: P 200 mg kg^{-1}, Na 20 mg kg^{-1}, Sr 4 mg kg^{-1}, Zn 0.7 mg kg^{-1}, Ba 0.05 mg kg^{-1} and Pb 0.03 mg kg^{-1}.

Table 6 Elemental contents in phosphate and oxalate matrix of urolith no. 11605 obtained by LA-ICP-MS and EMP analysis.

Element	Phosphate area					Oxalate area				
	Median content range	Arithmetic mean of median Contents	SD	Variability in content MAD	Arithmetic mean content	Median content range	Arithmetic mean of median contents	SD	Variability in content MAD	Arithmetic mean content
	LA-ICP-MS				EMP	LA-ICP-MS				EMP
	mg kg^{-1}			%	mg kg^{-1}	mg kg^{-1}			%	mg kg^{-1}
P	17.5–19.4 [a]	18.36 [a]	0.80 [a]	32	17.39 ± 0.22 [a]	1342–1489	1405	61	65	2400 ± 1200
Na	0.56–0.79 [a]	0.68 [a]	0.12 [a]	74	0.93 ± 0.06 [a]	694–973	840	148	51	870 ± 330
Sr	244–262	251.7	7.8	71	<LOD	39–41	39.8	1.2	82	<LOD
Zn	2303–3791	2890	630	47	2740 ± 630	26–43	32.4	7.1	44	<LOD
Ba	7–30	23	11	49	<LOD	2–11	8.3	4.0	55	<LOD
Pb	26–59	39	18	76	<LOD	1–3	2.15	0.98	63	<LOD

[a] %$_{m/m}$

22

Fig. 6 Distributions of a) $^{44}Ca^+$ and of elemental contents of b) P, c) Na, d) Sr, e) Zn, f) Ba and g) Pb which were quantified using the single-point calibration with pellet no. 9130.

23
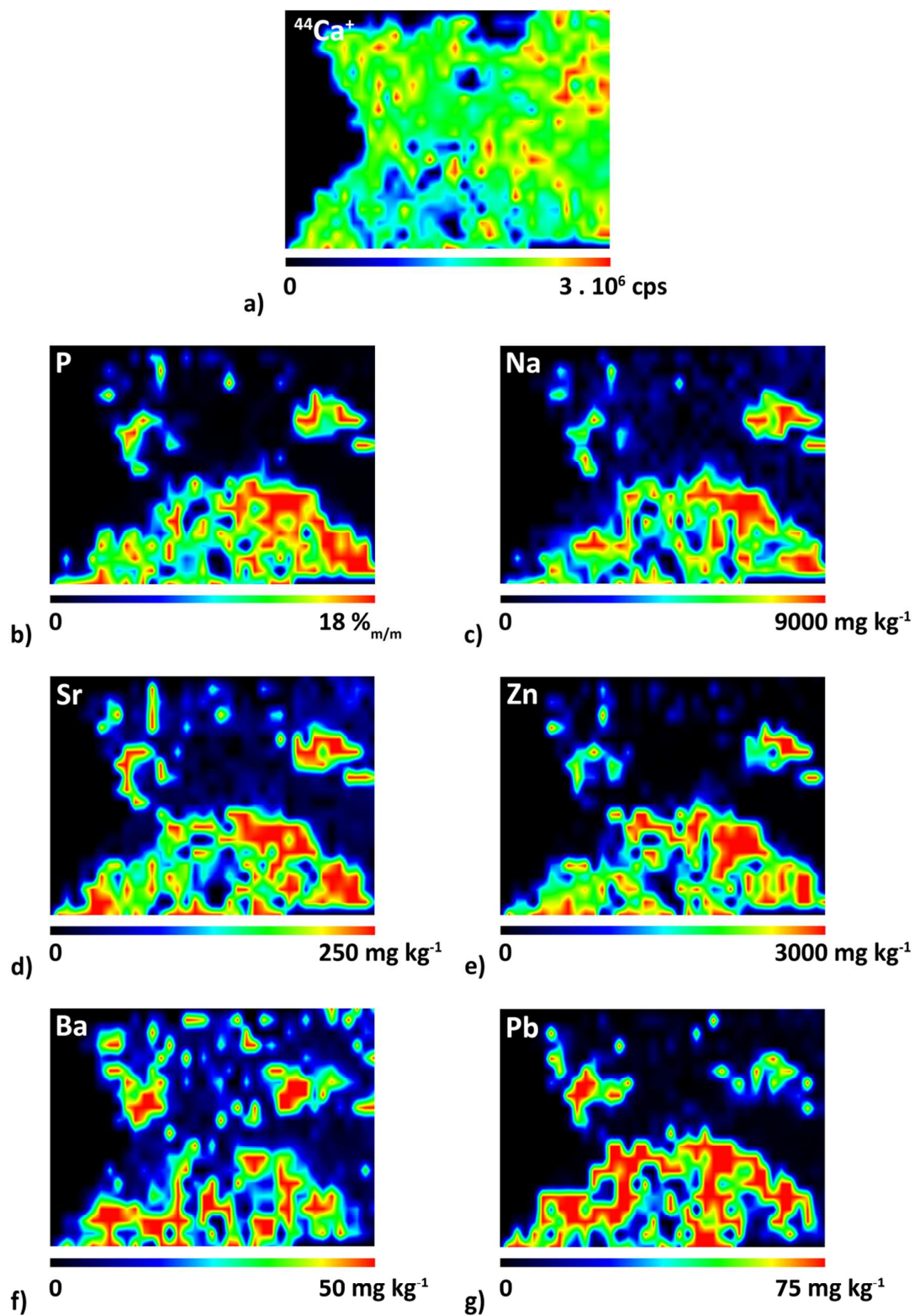
Conclusions

The kidney stone investigation plays important role in medical treatment when the process of formation and growth of uroliths as well as the influence of environmental pollution, for instance, have to be known. In this study, new flexible matrix-matched calibration was designed, tested and used to quantify distribution of elements in uroliths by laser ablation inductively coupled plasma mass spectrometry. Two-dimensional distributions of isotopic signals obtained from the selected area of the urolith section surface were converted to maps of elemental contents using the matrix-matched calibration. Calibration kits comprising 9 – 15 pressed pellets (depending on a particular element) were tested for homogeneity, signal stability and linear response with satisfactory results. Pellets were prepared without any binder from powdered uroliths consisting of phosphate, oxalate and urate phases. Despite the fact that the individual calibration pellets differ significantly in proportions of mineral phases and therefore also in physical and physico-chemical properties, linear calibration model in the range of three orders of magnitude and with zero intercept was obtained for P, Na, Mg, Zn, Ba and Pb. Low scatter of calibration points is characterized by coefficients of determination > 0.9955 and narrow confidence and prediction bands. This tight correlation was achieved through internal standardization. Correction of isotopic signals for different ablation rates in phosphate, oxalate and urate matrices of calibration pellets was successfully accomplished by internal standardization with response factor of $^{44}Ca^+$. For this purpose, calcium contents in particular uroliths employed for preparation of calibration pellets were determined by solution analysis, while average content of calcium in oxalate and phosphate phases of mapped urolith section surface was determined by electron microprobe.

To reduce the time of analysis, the four-point and four single-point calibrations were tested by analysis of pressed pellet of bone meal NIST SRM 1486. The four-point calibration with coefficient of determination in the range of 0.990-0.999 and single-point calibrations with phosphate matrix pellets yielded better trueness in comparison with oxalate pellet. This proved feasibility of quantification of elemental maps using calibration with a single pellet. Trueness of quantitative elemental maps obtained by LA-ICP-MS was indirectly proved by comparison of averaged elemental contents in phosphate/oxalate phases with those determined by electron microprobe. Limits of detection of minor or trace elements (Sr, Zn, Pb, and Ba) calculated from standard error of regression (calibration) were found to be between units and hundreds of mg kg^{-1}.

The proposed calibration exhibits advantages over using the bone meal NIST SRM 1486. Unlike this SRM, calibration samples prepared from uroliths cover existing wide range of elemental contents in analyzed samples without extrapolation, which is on the other hand unavoidable in case of Na, Mg, K, Pb, Sr and Zn quantification using NIST 1486. Number of calibration standards can be flexibly adapted to elemental contents in a particular urolith. Besides P, Na, Mg, Zn, Ba and Pb, urolith pressed pellets can also encompass linear multi-point calibrations for C, K, Al, Mn, Fe, Cu, Rb and Sn, while NIST SRM 1486 covers only Ca, Mg, P, Fe, K, Pb, Sr, and Zn with certified values. However, real content of K, Pb, Sr, and Zn in analyzed uroliths is frequently above particular certified values.

Acknowledgements

References

1. M. Debeljak, J. T. van Elteren and K. Vogel-Mikus, *Anal. Chim. Acta*, 2013, **787**, 155-162.
2. A. Hanc, A. Piechalak, B. Tomaszewska and D. Baralkiewicz, *Int. J. Mass Spectrom.*, 2014, **363**, 16-22.
3. M. Galiova, J. Kaiser, K. Novotny, M. Hartl, R. Kizek and P. Babula, *Microsc. Res. Techniq.*, 2011, **74**, 845-852.
4. A. Kötschau, G. Büchel, J. W. Einax, C. Fischer, W. von Tümpling and D. Merten, *Microchem. J.*, 2013, **110,** 783-789.
5. S. R. Ellis, A. L. Bruinen and R. M. A. Heeren, *Anal. Bioanal. Chem.*, 2014, **406,**1275-1289.
6. J. Koelmel, T. Leland and H. Wang, *Environ. Pollut.*, 2013, **174**, 222-228.
7. A. Hanc, I. Komorowicz, M. Iskra, W. Majewski and D. Baralkiewicz, *Anal. Bioanal. Chem.*, 2011, **399**, 3221-3231.
8. S. Gruhl, F. Witte, J. Vogt, Juergen and C. Vogt, *J. Anal. Atom. Spectrom.*, 2009, **24**, 181-188.
9. J. Chou, C. Austin, P. Doble, B. Ben-Nissan and B. Milthorpe, *J. Tissue Eng. Regen. M.*, 2014, **8**, 515-520.
10. E. G. Grosch, J. Kosler, N. McLoughlin, K. Drost and J. Slama, *Precambrian Res.*, 2011, **191**, 85-99.
11. C. M. Fisher, H. P. Longerich, S. E. Jackson and J. M. Hanchar, *J. Anal. Atom. Spectrom.*, 2010, **25**, 1905-1920.
12. M. Bertini, A. Izmer, F. Vanhaecke and E. M. Krupp, *J. Anal. Atom. Spectrom.*, 2013, **28**, 77-91.
13. A. Nevin, G. Spoto and D Anglos, Demetrios, *Appl. Phys. A-Mater.*, 2012, **106**, 339-361.
14. C. Chataigner, M. Isikli, B. Gratuze and V. Cil, *Archaeometry*, 2014, **56**, 351-374.
15. C. Stadlbauer, C. Reiter, B. Patzak, G. Stingeder and T. Prohaska, *Anal. Bioanal. Chem.*, 2007, **388**, 593-602.
16. T. Prohaska, C. Latkoczy, G. Schultheis, M. Teschler-Nicola and G. Stingeder, *J. Anal. Atom. Spectrom.*, 2002, **17**, 887-891.
17. M. Vasinova Galiova, M. Nyvltova Fisakova, J. Kynicky, L. Prokes, H. Neff, A. Z. Mason, P. Gadas, J. Kosler and V. Kanicky, *Talanta*, 2013, **105**, 235-243.
18. A. E. Dolphin and A. H. Goodman, *Am. J. Phys. Anthropol.*, 2009, **140**, 399-409.
19. A. E. Dolphin, A. H. Goodman and D. D. Amarasiriwardena, *Am. J. Phys. Anthropol.*, 2005, **128**, 878-888.
20. D. Hare, C. Austin, P. Doble and M. Arora, *J. Dent.*, 2011, **39**, 397-403.
21. A. Arvidsson, B. Liedberg, K. Moller, B. Lyven, A. Sellen and A. Wennerberg, *J. Dent.*, 2002, **30**, 67-75.
22. Z. A. Doubleday, C. Izzo, Christopher, S. H. Woodcock and B. M. Gillanders, *Aquat. Biol.*, 2013, **18**, 271-280.
23. A. D. Clarke, K. H. Telmer and J. M. Shrimpton, *Ecol. Freshw. Fish*, 2007, **16**, 354-361.
24. B. Wu and J. S. Becker, J. Sabine, *Int. J. Mass Spectrom.*, 2012, **323**, 34-40.
25. S. D. Urgast, D. G. Ellingsen, B. Berlinger, E. Eilertsen, G. Friisk, V. Skaug, Y. Thomassen, J. H. Beattie, I. Kwun and J. Feldmann, *Anal. Bioanal. Chem.*, 2012, **404**, 89-99.
26. O. Reifschneider, C. A. Wehe, I. Raj, J. Ehmcke, G. Ciarimboli, M. Sperling and U. Karst, *Metallomics*, 2013, **5**, 1440-1447.
27. D. Drescher, C. Giesen, H. Traub, U. Panne, J. Kneipp and N. Jakubowski, *Anal. Chem.*, 2012, **84**, 9684-9688.
28. L. Prien and C. Frondel, *J. Urol.*, 1947, **57**, 949-994.

29. M. L. Stoller and M. V. Meng, Urinary stone disease: the practical guide to medical and surgical management, Humana press, New Jersey, 2007.

30. N. Mandel, *Lab. Med.*, 1986, **17,** 449-458.

31. S. Tamosaityte, V. Hendrixson, A. Zelvys, R. Tyla, Z. A. Kucinskiene, F. Jankevicius, M. Pucetaite, V. Jablonskiene and V. Sablinskas, *J. Biomed. Opt.*, 2013, **18**.

32. C. Conti, M. Casati, C. Colombo, M. Realini, L. Brambilla and G. Zerbi, *Spectrochim. Acta A*, 2014, **128**, 413-419.

33. R. Selvaraju, A. Raja and G. Thiruppathi, *Spectrochim. Acta A*, 2013, **114**, 650-657.

34. S. D. Blaschko, J. Miller, T. Chi, L. Flechner, S. Fakra, A. Kahn, P. Kapahi and M. L. Stoller, *J. Urology*, 2013, **189**, 726-734.

35. K. Kaneko, Y. Matsuta, M. Moriyama, M. Yasuda, N. Chishima, N. Yamaoka, T. Fukuuchi, K. Miyazawa and K. Suzuki, *Int. J. Urol.*, 2014, **21**, 341-346.

36. E. S. Wisenbaugh, R. G. Paden, A. C. Silva and M. R. Humphreys, *Urology*, 2014, **83**, 1243-1247.

37. V. Uvarov, I. Popov, N. Shapur, T. Abdin, O. N. Gofrit, D. Pode and M. Duvdevani, *Environ. Geochem. Hlth.*, 2011, **33**, 613-622.

38. B. G. Oztoprak, J. Gonzalez, J. Yoo, T. Gulecen, N. Mutlu, E. E. Russo, O. Gundogdu and A. Demir, *Appl. Spectros.*, 2012, **66**, 1353-1361.

39. J. Anzano and R. J. Lasheras, *Talanta*, 2009, **79**, 352-360.

40. K. Stepankova, K. Novotny, M. Vasinova Galiova, V. Kanicky, J. Kaiser and D. W. Hahn, *Spectrochim. Acta B*, 2013, **81**, 43-49.

41. M.A. Chaudhri, J. Watling and F. A. Khan, *J. Radioanal. Nuc. Ch.*, 2007, **271**, 713-720.

42. M. Vasinova Galiova, R. Copjakova, R. Skoda, K. Stepankova, M. Vankova, J. Kuta, L. Prokes, J. Kynicky and V. Kanicky, *Spectrochim. Acta B*, 2014, **100**, 105-115.

43. A. Izmer, D. Gholap, K. De Houwer, F. Cuyckens and F. Vanhaecke, *J. Anal. Atom. Spectrom.*, 2012, **27**, 413-418.

44. H. J. Stärk and R. Wennrich, *Anal. Bioanal. Chem.*, 2011, **399**, 2211-2217.

45. X E. Moreno-Gordaliza, C. Giesen, A. Lazaro, D. Esteban-Fernandez, B. Humanes, B. Canas, U. Panne, A. Tejedor, N. Jakubowski and M.M. Gomez-Gomez, *Anal. Chem.*, 2011, **83**, 7933-7940.

46. D. J. Hare, J. Lear, D. Bishop, A. Beavis and P.A. Doble, *Anal. Method.*, 2013, **5**, 1915-1921.

47. D. Tabersky, N. A. Luechinger, M. Rossier, E. Reusser, K. Hametner, B. Aeschlimann, D. A. Frick, S. C. Halim, J. Thompson, L. Danyushevsky and D. Guenther, *J. Anal. Atom. Spectrom.*, 2014, **29**, 955-962.

48. I. Hubova, M. Hola, , J. Pinkas and V.Kanicky, *J. Anal. Atom. Spectrom.*, 2007, **22**, 1238-1243.

49. H. Sela, Z. Karpas, H. Cohen, Y. Zakon and Y. Zeiri, *Inter. J. Mass Spectrom.*, 2011, **307**, 142-148.

50. J. A. T. Pugh, A. G. Cox, C. W. McLeod, J. Bunch, B. Whitby, B. Gordon, T. Kalber and E. White, *J. Anal. Atom. Spectrom.*, 2011, **26**, 1667-1673.

51. J. Kuta, J. Machát, D. Benova, R. Červenka and T. Kořistková, *Cent. Eur. J. Chem.*, 2012, **10**, 1475-1483.

52. J. L. Pouchou, F. Pichoir, "PAP", Procedure for Improved Quantitative Microanalysis. In Armstrong JT (ed.) Microbeam Analysis Proc. San Francisco Press, San Francisco, 1985, pp 104-106.

53. J. Kuta, J. Machat, D. Benova, R. Cervenka, J. Zeman and P Martinec, *Environ. Geochem. Hlth*, 2013, **35**, 511-522.

54. http://georem.mpch-mainz.gwdg.de/sample_query.asp (16/10/2014).